

Article

Lateral Ultimate Capacity of Monopile Foundations for Offshore Wind Turbines: Effects of Monopile Geometry and Soil Stiffness Properties

Yazeed A. Alsharedah ^{1,*}, Timothy Newson ² , M. Hesham El Naggar ²  and Jonathan A. Black ³

¹ Department Civil Engineering, College of Engineering, Qassim University, King Abdulaziz rd., Qassim 52571, Saudi Arabia

² Civil and Environmental Engineering Department, Western University, London, ON N6A 3K7, Canada; tnewson@eng.uwo.ca (T.N.); naggar@uwo.ca (M.H.E.N.)

³ Civil and Environmental Engineering Department, Queen's University at Belfast, Belfast BT7 1NN, UK; j.black@qub.ac.uk

* Correspondence: y.alsharredah@qu.edu.sa

Abstract: Offshore Wind Turbines (OWT) with increasingly higher energy output are being developed to meet energy demands, posing greater challenges for their foundation design. Several foundation types are used to support these turbines, with monopiles (MPs) accounting for 80% of the installed capacity. In this study, three-dimensional (3D) nonlinear finite element models (FEM) were employed to investigate the behaviour of a monopile foundation supporting a 5MW wind turbine subjected to lateral loading. The results indicate that the MP behaviour depends on the pile length to diameter (L/D) ratio and the soil shear strength. Inspection of the bending-moment profiles at the lateral ultimate capacity indicated that the monopiles can behave in a flexible manner, even with low L/D ratios. The L/D ratio affected the MP normalized lateral ultimate capacity to varying degrees, and the biggest effect was for soft clays, amounting to an approximately five-fold increase for L/D values of 3.33 to 13.33. Lesser effects were found for stiff clays.

Keywords: monopile; offshore wind turbines (OWT); lateral ultimate capacity; green energy



Citation: Alsharedah, Y.A.; Newson, T.; El Naggar, M.H.; Black, J.A.

Lateral Ultimate Capacity of Monopile Foundations for Offshore Wind Turbines: Effects of Monopile Geometry and Soil Stiffness Properties. *Appl. Sci.* **2023**, *13*, 12269. <https://doi.org/10.3390/app132212269>

Academic Editors: Rongquan Wang, Robert Mayon and Yingyi Liu

Received: 27 August 2023

Revised: 29 October 2023

Accepted: 30 October 2023

Published: 13 November 2023



Copyright: © 2023 by the authors. Licensee MDPI, Basel, Switzerland. This article is an open access article distributed under the terms and conditions of the Creative Commons Attribution (CC BY) license (<https://creativecommons.org/licenses/by/4.0/>).

1. Introduction

Sustainable energy sources such as wind, hydro and solar are critical for the planet and are currently underutilized. Global warming, increasing CO₂ in the atmosphere and fears of increasing frequency and severity of natural disasters such as extreme weather, flooding and tsunamis have driven government bodies, research institutes and industry to move at an increased pace towards cultivating more energy from these sources, in a bid to reduce dependency on fossil fuels. Specifically, exponential growth of wind energy has been achieved from onshore and offshore wind farms (OWF), with individual offshore wind turbines (OWTs) with a capacity of 14 MW reaching the market [1]. Figure 1 shows the energy output from offshore wind farms in Europe between 2000–2020. This increase in capacity has been realized using heavier and taller turbines, often leading to very large foundation systems, which can constitute up to 40% of the total cost [2–4].

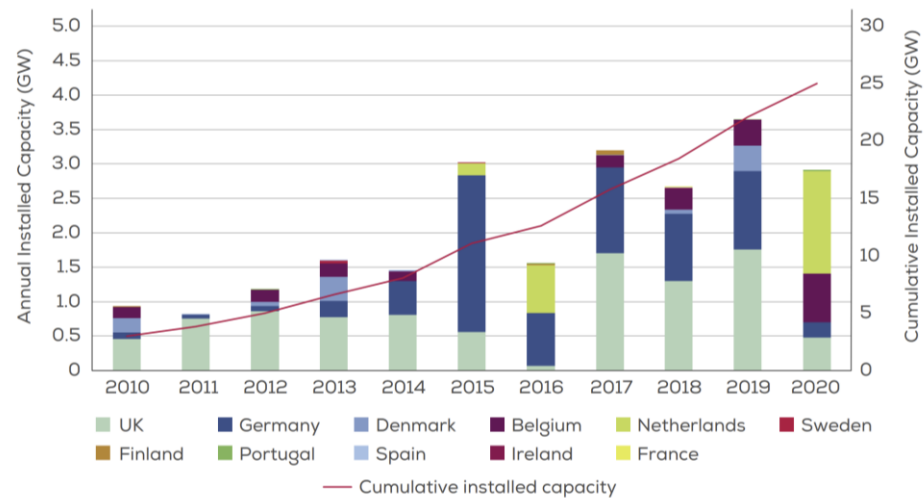


Figure 1. Capacity of wind farms installed in Europe [5].

Different foundation systems are employed to support wind turbines, such as fixed gravity base foundations (GBF), tripod structures, jackets, suction caissons, monopiles (MP) and buoyant fixed structures [6–9]. Figure 2 presents some of the foundation systems currently used to support OWT. The foundation-design process is iterative in nature and begins with an estimate of the lateral applied loads from the wind, waves and currents, in addition to the aerodynamic forces. Since the geometry of the foundation is unknown, the size is usually assumed initially and then the foundation response is evaluated. If the assumed foundation geometry is insufficient to meet the ultimate or serviceability limit states, a new geometry is assumed. This loop repeats itself until a suitable foundation geometry is found [3].

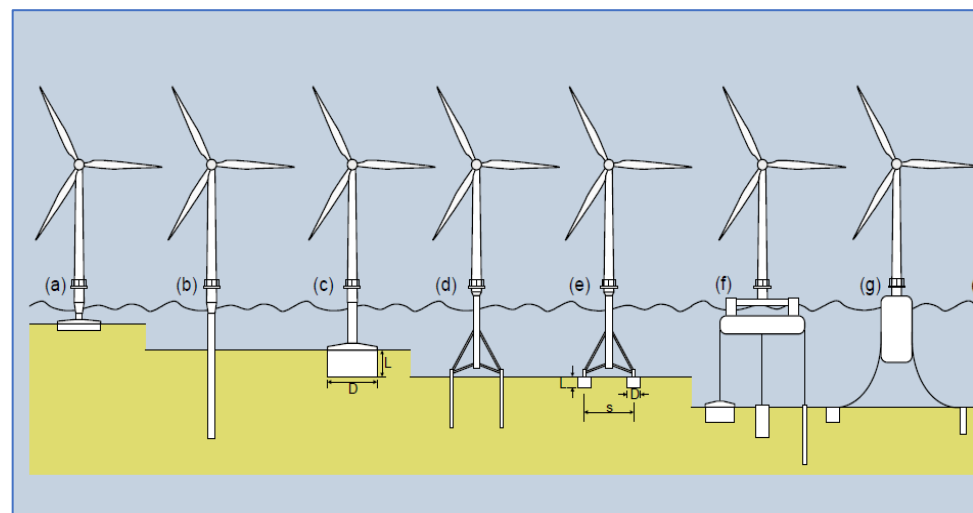


Figure 2. Available foundation options for offshore wind turbines. (a) GBF, (b) monopile, (c) suction caisson, (d) tripod/tetrapod piles, (e) tripod/tetrapod suction caissons, (f) multiple foundation options, and (g) guys with anchors [10].

Extensive records of the performance of monopiles from other offshore structures, such as oil platforms, have aided engineers with the design of early forms of OWTs. For these piles, the design is based on the famous p - y curve approach [10–14]. In this approach, the soil layers are replaced with independent springs, each having a different load–displacement curve, known as the p - y curve. This approach was first proposed by [12] and validated by [15], for the case of a slender pile in soft soil, and then by [16] who proposed the p - y formulae for stiff soils. However, a few issues have been raised

when applying this method to offshore wind turbines. Firstly, the p–y approach was validated [15] by testing slender piles in soft soil with a diameter of only 0.32 m and a length of 12.8 m, giving an L/D ratio of 39.5. However, a typical offshore wind turbine has an order of magnitude of a larger diameter monopile with a lower L/D ratio. Numerous researchers have pointed out that diameter effects were not included in the original method (e.g., [10,17–22]). Secondly, other deficiencies arise from the fact that the tested pile only experienced 20 cycles of loading, whereas the expected number of load cycles experienced by an OWT in its lifetime can be of the order of 10^7 . Thirdly, the ratio of vertical load to lateral load for oil and gas platforms is much higher than that for wind turbines, making direct application of current American Petroleum Institute (API) recommendations for monopile design questionable. Finally, the effect of cyclic loading is treated uniformly along the pile depth with a reduction factor A of 0.9, irrespective of load level [23]. Improved p–y formulae have since focused on closing these gaps in the literature, such as the recent PISA project. The PISA project created an improved version of the p–y approach, where additional resistance is added from the side and base friction [10,17,22]. For instance, ref. [20] conducted nine centrifuge tests on monopiles installed in kaolin clay, which were subjected to monotonic and cyclic loading. The results demonstrated that the API p–y curves of [15] underestimated the stiffness properties of the monopiles, and the displacement and rotation under cyclic loading depended on the number of load cycles and cyclic load amplitude, which is not accounted for in the current API p–y approach. Ref. [22] conducted field tests on large-diameter open-ended driven piles in soft clay of offshore China. Their tests involved driving a monopile of 2.2 m diameter into soft clay, and the piles were subjected to both monotonic and low-frequency cyclic lateral loading. Their results showed that the API p–y curves underestimated both initial stiffness and ultimate capacity, possibly due to reconsolidation from pile driving, which supports the results of [20,24]. They proposed a hyperbolic function for the p–y curves, which provided an excellent match to the field-test results. Additionally, their p–y curves included a degradation factor, t , as a function of depth and cyclic-load level. Other methods to obtain the lateral ultimate capacity and deflection at the mudline of monopiles include physical testing, FE modelling or Bender’s approach (e.g., [6,8,14,23,25–33]).

While the lateral behaviour of monopiles has been investigated widely, there is currently no easily available way to deduce the pile capacity. Hence, using a new normalization approach for monopiles for OWTs, the authors are hopeful the new approach can be beneficial and insightful for OWT monopile design. The results obtained from this study can also verify the results from Beam on Nonlinear Winkler Foundation (BNWF) analyses, and benchmark new FEM results helping decision making for future developments of sustainable energy.

1.1. Methodology

The aim of this research is to establish a quick method for estimating monopile lateral ultimate capacity based on a few soil parameters and design inputs. This has been accomplished by studying monopile behavior under eccentric lateral loading similar to that of a 5 MW wind turbine in medium-depth water. To do so, several prototype dimensions of MP models were established. A series of finite element models employing displacement-controlled loading were conducted. Model responses were evaluated for their bending behaviour and lateral ultimate capacity. A new normalization study examines whether the lateral capacity of the pile can be characterized primarily using the L/D ratio, as a combination of L/D and normalized stiffness of the monopile with respect to the soil. The effects of footing rigidity on the lateral ultimate capacity of monopiles’ foundations is studied by changing the ground conditions, and generic curves are established relating to the ultimate lateral capacity of the foundation with respect to L/D and the foundation’s normalized stiffness E_p^* given by the following:

$$E_p^* = \frac{E_p I_p}{I_{scp}} \quad (1)$$

E_p^* : normalized stiffness of the monopile; E_p : pile Young’s modulus; I_p : pile moment of inertia; and I_{scp} : moment of inertia of a solid cross-section pile of same diameter as the actual pile.

Specifically, we investigate the mode of contribution using a normalization procedure of the ultimate capacity of a monopile considering the effects of soil profile and pile/soil relative rigidity given using E_p^*/E_{50} , where E_p^* is the foundation normalized stiffness and E_{50} is the soil Young’s modulus at 50% of the ultimate deviatoric load is that causing failure of a soil specimen in a triaxial apparatus, q_f . This approach enables the normalization of the lateral ultimate capacity by the soil shear strength and pile diameter. Design charts are established to develop the MP lateral ultimate capacity considering L/D and E_p^*/E_{50} ratios for a given eccentricity. Finally, predictive equations are proposed to calculate the MP lateral ultimate capacity based on best-fit data from finite element (FE) results. The normalization method used provides a pathway for use of the same framework with other eccentricities.

Three-dimensional (3D) FE models (FEMs) were conducted to simulate the MP foundations. Tetrahedron 10-noded elements were used to discretize the soil, while plate elements were used to discretize the tower and the pile. The FEM was validated against the results of field tests from [22], and the pile was simulated using embedded beam elements confined with solid elements instead of plate elements, to enable the evaluation of the structural forces. To account for slippage and gap formation, 6-noded interface elements were used to simulate contact between the solid (pile) zone and soil. The strength of the interface elements was defined through a reduction factor, R_{int} , applied to the soil properties, which varied between 1 and 0.3 for soft and stiff soils, respectively. The tower was simulated as a beam element having unit weight, diameter, E and thickness of 77 kN/m^3 , 6 m, 200 GPa and 0.035 m, respectively. It is rigidly connected to the surrounding solid elements to ensure that the load is transferred uniformly over the pile area. In all models, x and y boundaries were set at $7D$ from the model center and restricted to move horizontally, while being allowed to move vertically. The bottom, z , boundary was fixed and placed at least $3D$ below the pile tip to avoid any boundary effects and to model rotational stiffness correctly. The FEM had an average of 25,000 elements.

The soil behaviour was simulated employing the hardening-soil (HS) model obeying the Mohr–Coulomb (MC) failure criterion [34]. The HS model can simulate the behaviour of both soft and stiff soils. This model is further divided into 2 options: undrained A, which considers stress-dependent elastic parameters, and undrained B, which does not account for the variation of the elastic parameters with changing overburden stress. In this study, the undrained A option has been chosen to consider changing stiffness of the soil with depth. Thus, the HS model with the undrained A option accounts for the stiffness stress dependency, allows plastic straining due to deviatoric and primary compression loading and can simulate the appropriate higher unloading stiffness, hence accounting for plastic straining before failure is reached. The clay behaviour is accounted for by considering the effects of two strain-hardening components; namely volumetric hardening (cap) and shear, where contraction and densification cause the yield surface to expand. The soil-stiffness parameters in the HS model can be determined as follows.

$$E_{oed} = E_{oed,ref} \left(\frac{c' \cos \phi' - \frac{\sigma'_3}{k_o^{NC}} \sin \phi'}{c' \cos \phi' + p'_{ref} \sin \phi'} \right)^m \tag{2}$$

$$E_{50} = E_{50,ref} \left(\frac{c' \cos \phi' - \sigma'_3 \sin \phi'}{c' \cos \phi' + p'_{ref} \sin \phi'} \right)^m \tag{3}$$

$$E_{ur} = E_{ur,ref} \left(\frac{c' \cos \phi' - \sigma'_3 \sin \phi'}{c' \cos \phi' + p'_{ref} \sin \phi'} \right)^m \tag{4}$$

where c' ϕ' are soil effective cohesion and friction angle. p'_{ref} is the references’ mean effective stress and m is an exponent defining the variation of the HS model parameters with depth. E_{oed} , and E_{ur} are the one dimensional oedometer modulus and unloading/reloading stiffness values.

The analysis involved four stages, including: The initial stage (initiation of geostatic stresses) in which equilibrium is established based on the lateral-earth-pressure coefficient at rest. k_0 is a construction stage in which all structures and interface elements are activated. Loading stages are where displacement-controlled loading is applied until failure is reached; and finally, the output stage where the structural forces and soil deformation are examined to establish the failure loads. In the FE model calculations, the lateral ultimate capacity was determined as either the maximum load at 3 m displacement of the tower head or the load causing yield stresses in the structural elements.

1.1.1. Validation

The FEM model benchmarking used a case study of field tests carried out on a 2.2 m diameter open-ended pile driven offshore in China [22]. The piles had a thickness of 0.03 m and a depth of 57.4 m below the seabed. Soil was characterised using a mechanical cone penetrometer (CPT) equipped with soundings for shear wave velocity. Cone penetration test, CPT, tip resistance, q_c , was converted to undrained shear strength, S_u , values using Equation (5):

$$S_u = 0.07q_c + 2 \quad (5)$$

The undrained shear strength profile was checked by retrieving soil samples and doing CIUC triaxial tests, and the results compare well with the S_u profile, validating the use of Equation (5).

Table 1 presents the soil properties established from the SCPT sounding and the model parameters utilized in the FEM of the field-test results.

Table 1. Calibrated Hs soil properties and model parameters for the case study.

Parameter	Clay1	Units
c'	15	kPa
Ψ	0	Degrees
ϕ'	8	Degrees
P'_{pop}	15	kPa
P'_{ref}	41	kPa
$e_{ini.}$	4.23	-
γ	17.9	KN/m ³
E_{oed}^{ref}	1406	kPa
E_{50}^{ref}	1758	kPa
E_{ur}^{ref}	5000	kPa
v_{ur}	0.2	-
m	0.6	-
PI	30	%
$K_{o,NC}$	0.86	-
R_f	0.9	-
Depth	0–5	m
Type of analysis	Undrained A	-

1.1.2. Convergence Study

Once the final set of soil parameters were defined, the convergence analysis was carried out. The purpose of this convergence analysis was to test the FE sensitivity to the model domain boundaries and to increase the accuracy of the results, defining the reference geometry and mesh size that will be followed in the parametric analysis. Figure 3 shows the dimensions studied herein, while Figure 4 displays a typical set of results for the convergence analysis, and in this case, the effects of the model vertical boundaries in the y direction (transverse direction of the loading, L_y) on the displacement at the mudline, u_m (m). The same procedure was followed to define the length of the model, L_x , and depth of the model, L_z (Figure 3). In all the analyses considered, the global element size was set to be medium sized, and a refinement zone extending 3D, 5D, and 7D away from the center

of the monopile and extending to the base of the model (zone of refinement in Figure 5) was investigated with changing coarseness factor (cf). This was completed to produce a finer mesh within the proximity of a monopile, where most of the strains were anticipated to take place. Based on the aforementioned convergence analyses, the selected boundary conditions are 7D for x, y from the pile centerline in all directions, with a refinement zone of 3D and cf of 0.2, yielding approximately 25,000 elements. This discretization of the domain provided good agreement with the practice reported by [35].

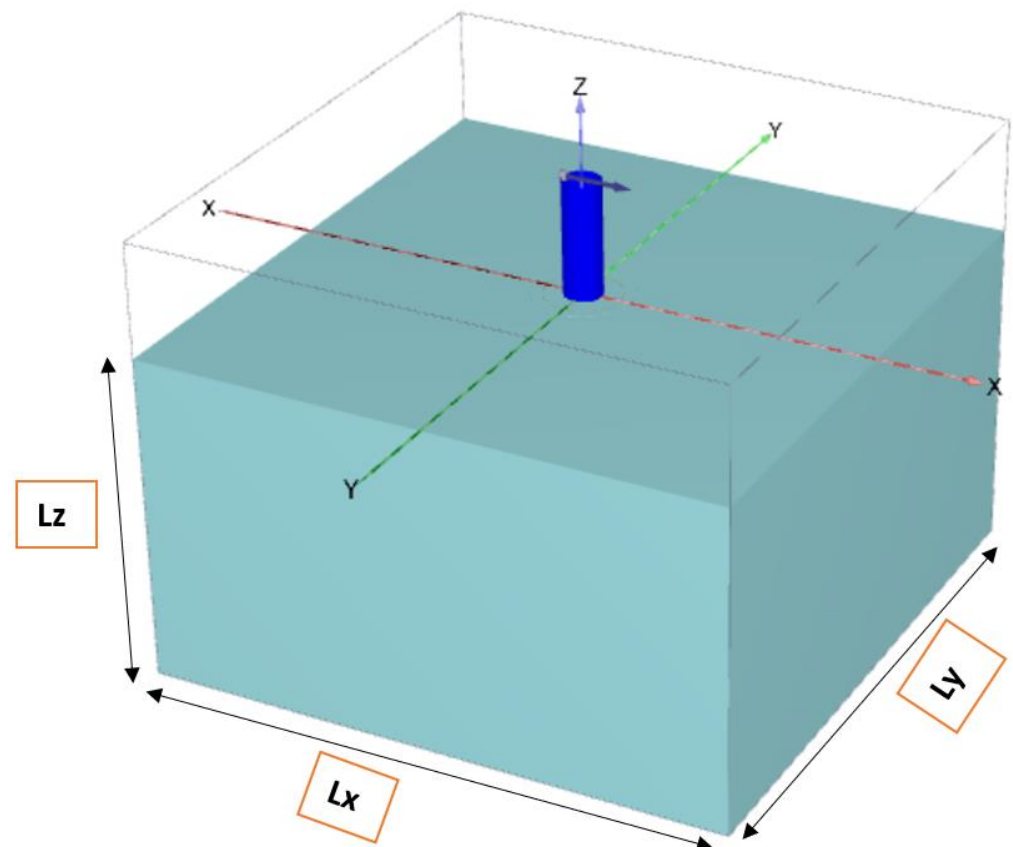


Figure 3. Boundary conditions varied in convergence analyses.

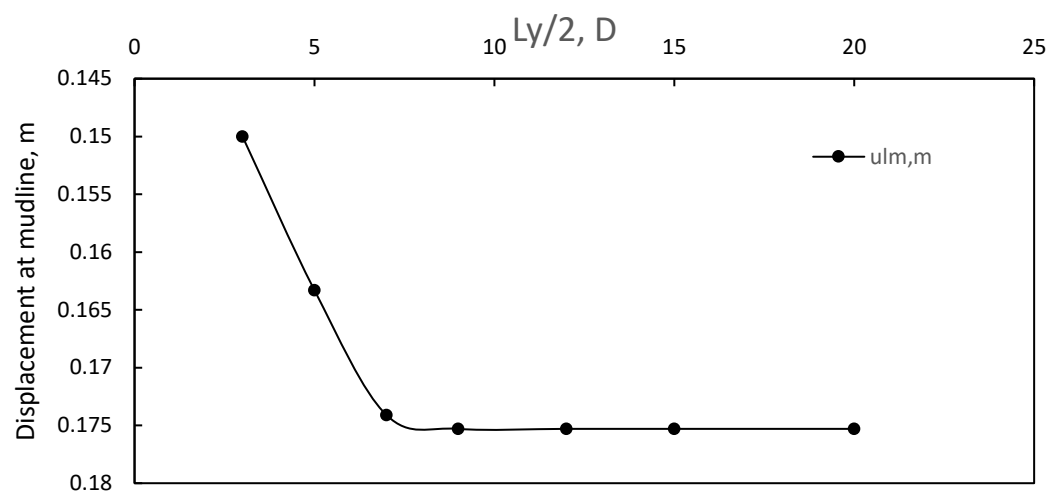


Figure 4. Sample of convergence analysis results.

Based on the results of the sensitivity analysis, the vertical boundaries were placed at 7D from the center of the model and the bottom boundary was placed more than (3D)

below the pile tip. The vertical boundaries were restricted horizontally and allowed to move vertically, while the bottom boundary was fixed in all directions (i.e., x , y , and z). These are standard model boundary conditions in Plaxis 3D and are used to remove any effects from the model boundaries on the structure response. The global mesh size was chosen to be medium sized after performing the sensitivity analysis, in which the FEM comprised 25,000 elements approximately. This was to ensure higher quality, yet time-efficient modeling. The mesh was further refined within a zone of $3D$ adjacent to the pile to increase the accuracy of the results. Figures 5 and 6 show a typical mesh used in the study.

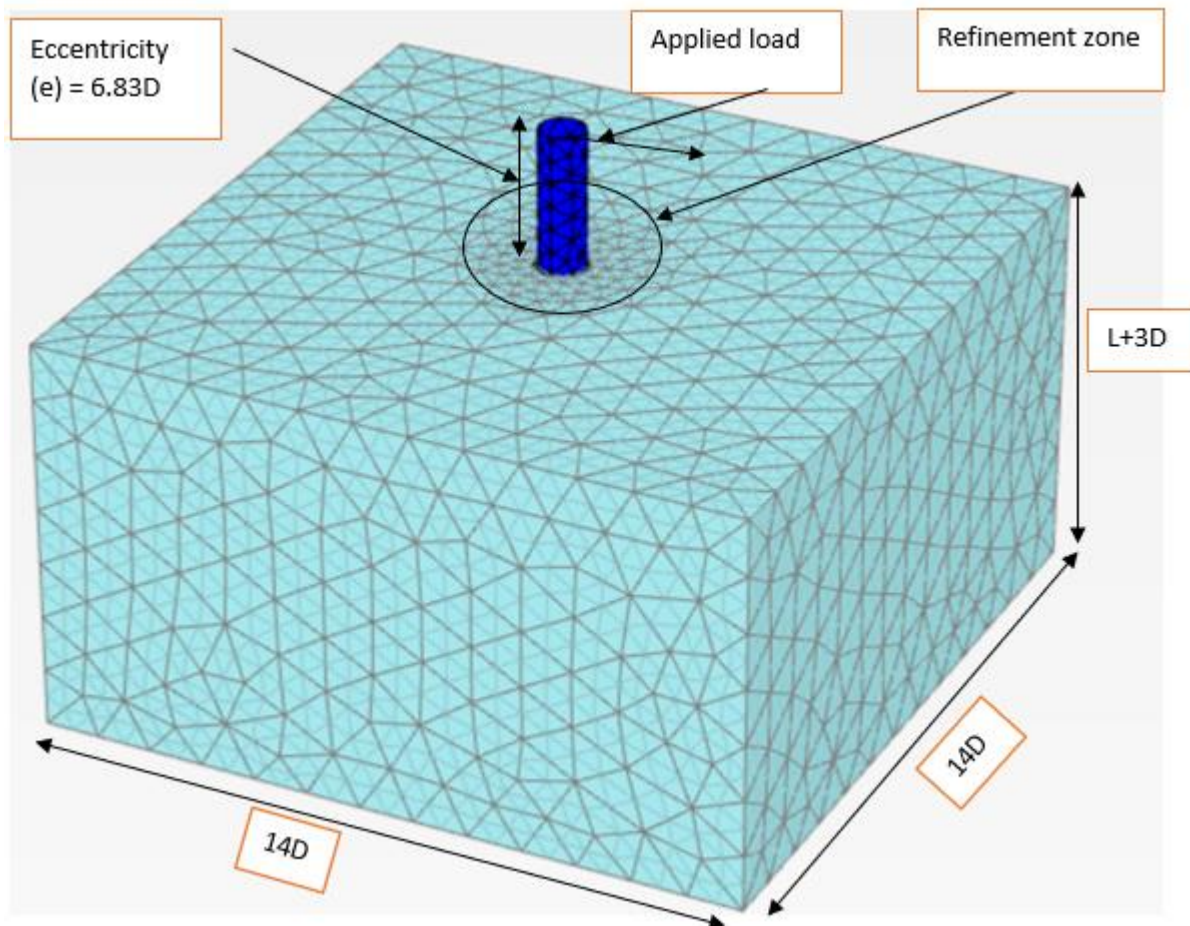


Figure 5. Developed mesh and location of lateral point load.

The load–displacement curve obtained from the FE analysis is plotted in Figure 7, along with the field data. Figure 7 demonstrates that there is excellent agreement between the calculated and measured load–displacement curves, validating the ability of the developed finite element model to simulate the behaviour of the large-diameter piles installed in the cohesive soil. Bending-moment and inclinometer data are also compared and excellent agreement is obtained as shown in Figure 8.

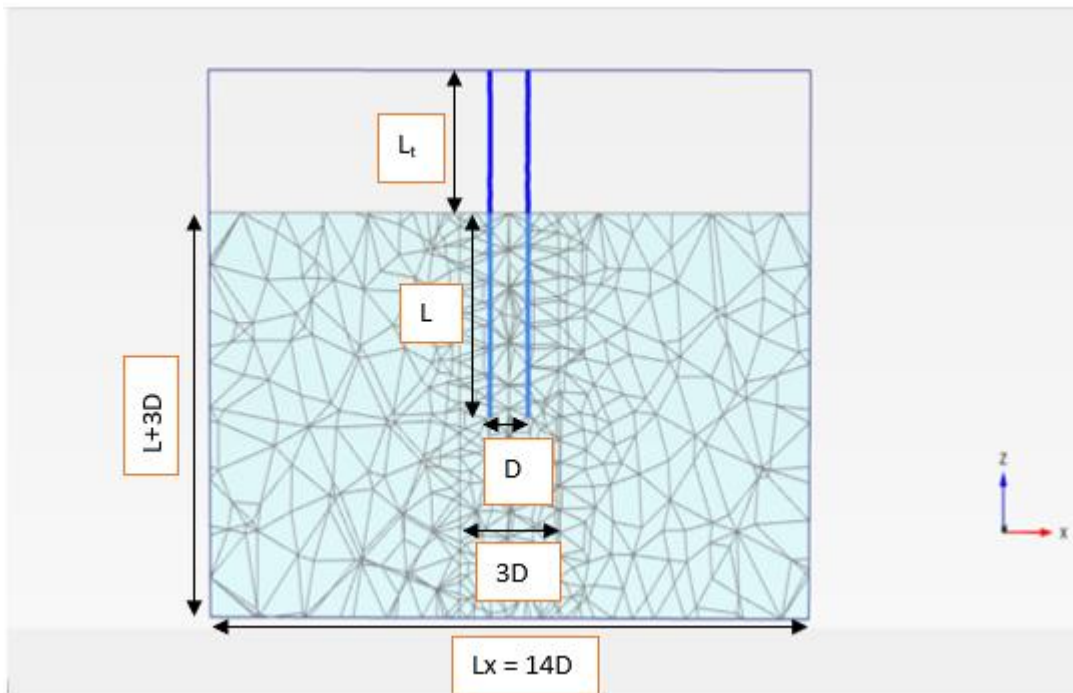


Figure 6. Cross section showing developed mesh.

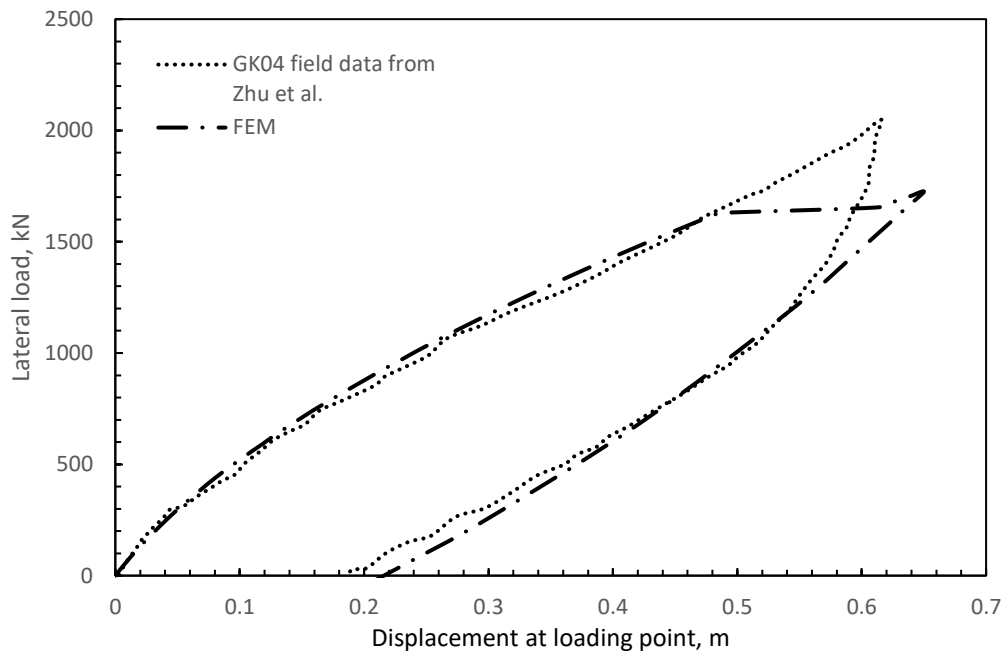


Figure 7. Load displacement curve using Hs undrained A parameters, GK04 field data from Zhu et al. [22].

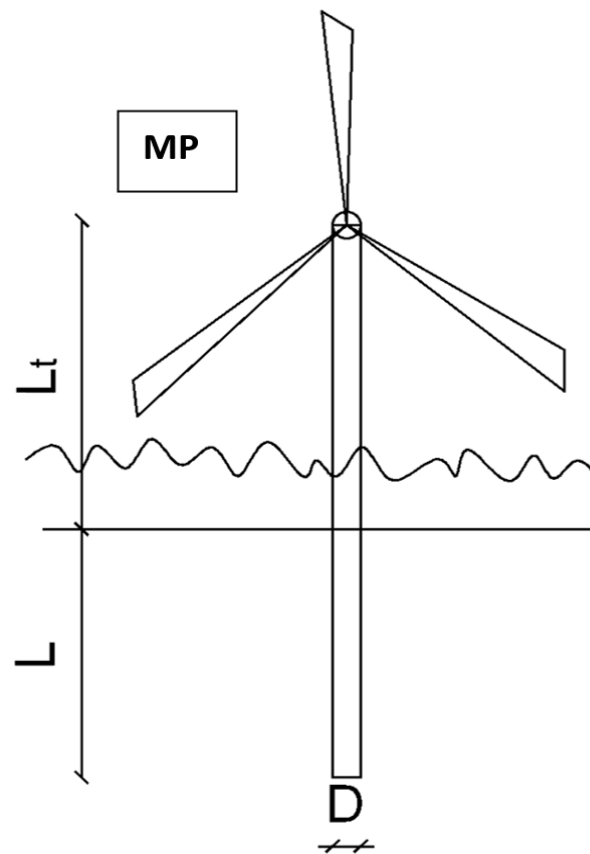


Figure 9. The considered monopile-foundation-system geometric notations (not to scale).

Table 3. Range of parameter analyses.

L , m	$L/D/(L_p/W)$	Foundation System	e/D_t	V , kN
20	3.33	Monopile	6.83	Own weight ¹
30	5		6.83	
40	6.67		6.83	
50	8.33		6.83	
60	10		6.83	
70	11.67		6.83	
80	13.33		6.83	

L : Depth of embedment; D : Pile's diameter; e : eccentricity of applied loads(m); D_t : Tower's diameter; and ¹: uniformly distributed.

Monopile Lateral Ultimate Capacity

The monopile lateral ultimate capacity may be governed by either the soil resistance or the pile's structural capacity. Hence, it was important to model the correct behavior of the soil and pile components. In Plaxis 3D, the pile can be modelled using either plate elements or embedded beam elements. However, both are assumed to behave elastically. While volume elements do not provide information on structural forces, embedded beam elements do provide structural forces and can be used to check whether the yield strength of the structural elements is reached. Ref. [36] indicated that by incorporating a solid zone around the pile, the embedded beam elements within solid elements behave like volume piles. Correspondingly, embedded beam elements within solid elements were utilized to simulate the piles, to enable proper evaluation of its ultimate capacity. The combined rigidity of both the solid elements and embedded beam elements was equivalent to that of the open-ended pile. To ensure beam elements would deflect with the solid elements, their Young's modulus E was divided by 10^6 . The resulting bending moment was then

multiplied by 10^6 to calculate the correct bending-moment value. Failure was determined to be either geotechnical or structural after examining output data and checking whether the applied load causes yielding conditions at the mudline. The lateral ultimate capacity is taken as the linear average between the two values on either side of the value that caused structural-capacity failure.

3. Results

The load displacement curves for monopiles in soft clay (clay1) and hard clay (clay6) are displayed in Figure 10. It can be seen that both the stiffness and strength increased with increasing L/D ratio in the soft clay indicating rigid pile behavior, Figure 10a. In the hard clay, a less discernible increase in stiffness is realized when using longer monopiles and the strength gain is also minimal due to the flexibility of the pile with respect to the soil, Figure 10b. Since the pile elements are considered to behave elastically, the load displacement curve is limited at the points where the flexural bending capacity is reached within the monopile, i.e., the load displacement curve is not valid beyond these points (shown in Figure 10 as square and diamond points). It can be noticed that in both clays this phenomenon occurs, although to a lesser extent in the soft clay.

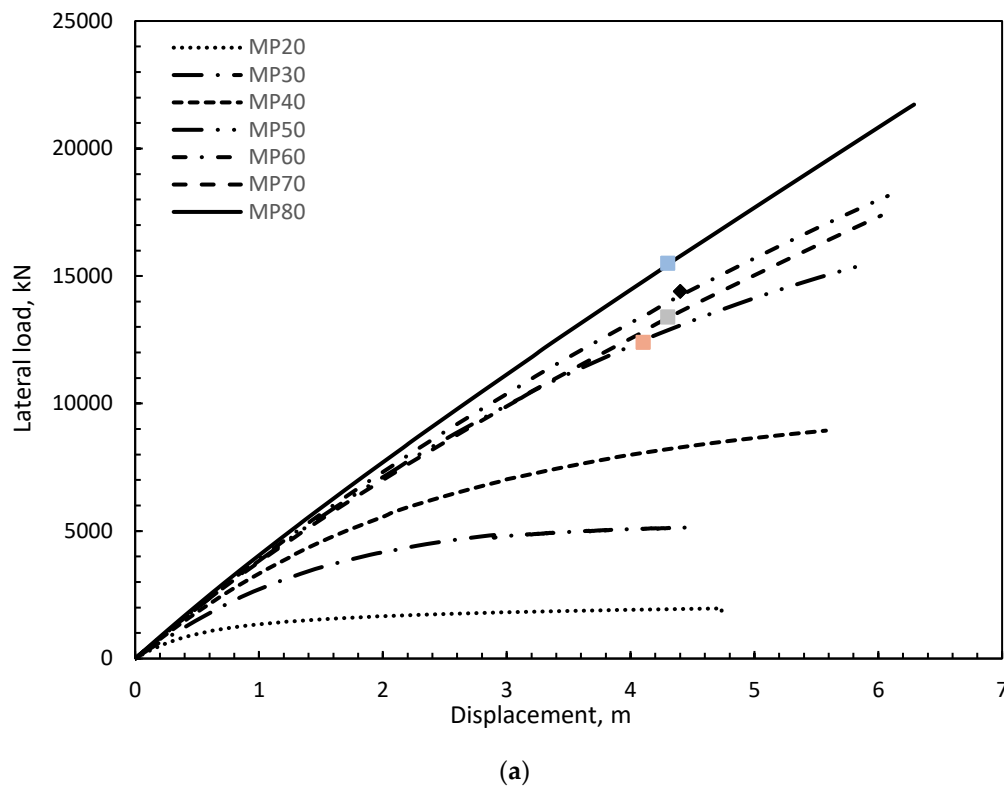


Figure 10. Cont.

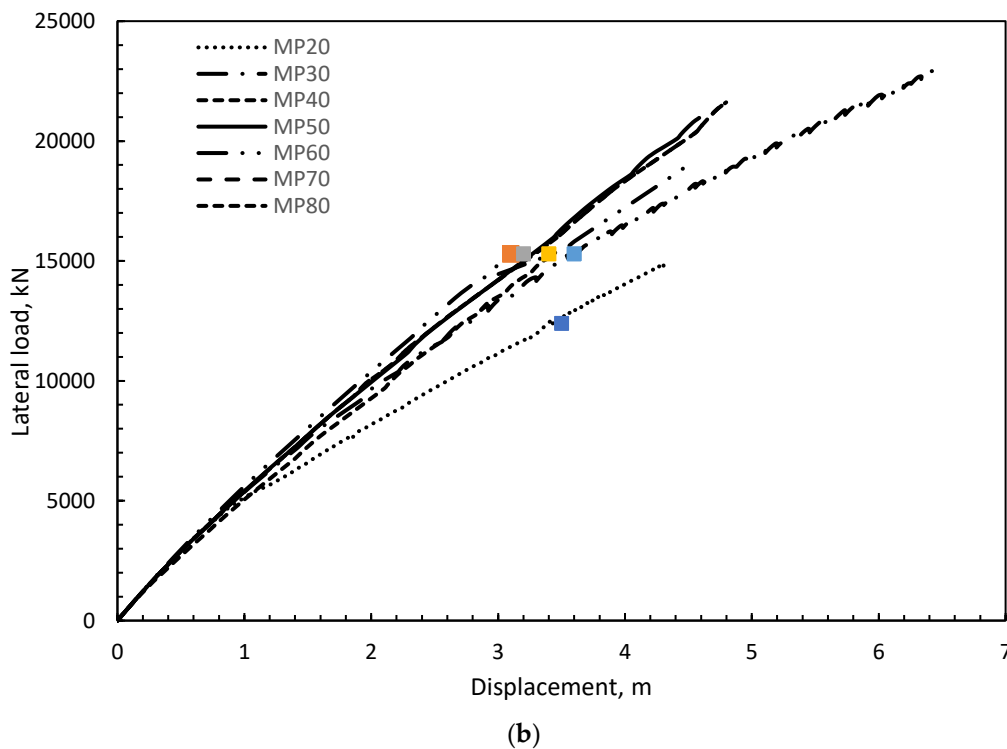


Figure 10. Load displacement curves of different lengths monopiles in (a) Clay1 and (b) Clay6.

4. Discussion

4.1. Discussion of Lateral Ultimate Capacity

Figure 11 presents the normalized ultimate capacity of the monopile versus the L/D ratio for various soil conditions (i.e., different normalized stiffness of the monopile models with respect to the soil). The normalized ultimate capacity of the monopile varies linearly with increase in normalized stiffness and reaches a plateau at E_p^*/E_{50} of 984 for cases of $L/D \leq 5$. For cases with $L/D > 5$, the normalized ultimate capacity showed a trilinear trajectory, noting there is a very wide range between E_p^*/E_{50} of 4536 and E_p^*/E_{50} of 10,322. Given the observed trends, the authors believe that they can be assumed to be linear.

For a given E_p^*/E_{50} ratio, the variation of monopiles' normalized ultimate capacity with different L/D ratios differs significantly between E_p^*/E_{50} of 10,250, where a 'rigid' response was observed for all L/D ratios, and for E_p^*/E_{50} , a value of 127 where a flexible pile response was observed. This can be explained by inspecting the variation of the normalized ultimate capacity versus L/D ratio for all soil profiles considered. Figure 11 shows that for a stiff to hard clay site (E_p^*/E_{50} of less than 499), the pile lateral capacity reached a maximum at a L/D ratio of between 5–8. For soft clay sites, the capacity continues to increase as L/D increases, Figure 12.

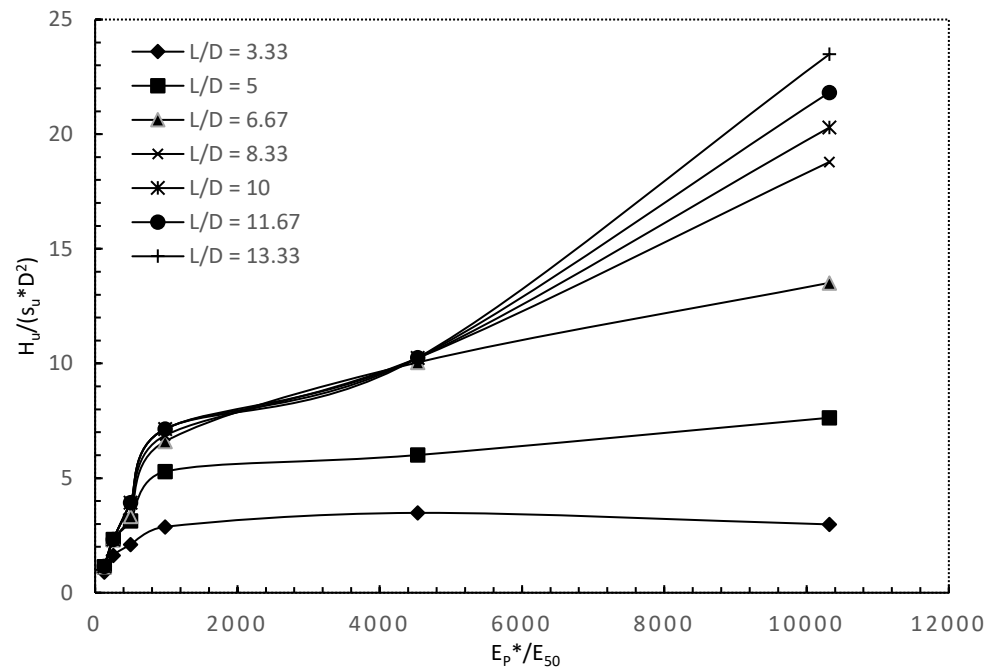


Figure 11. Effects of relative rigidity on normalized lateral ultimate capacity of the monopiles.

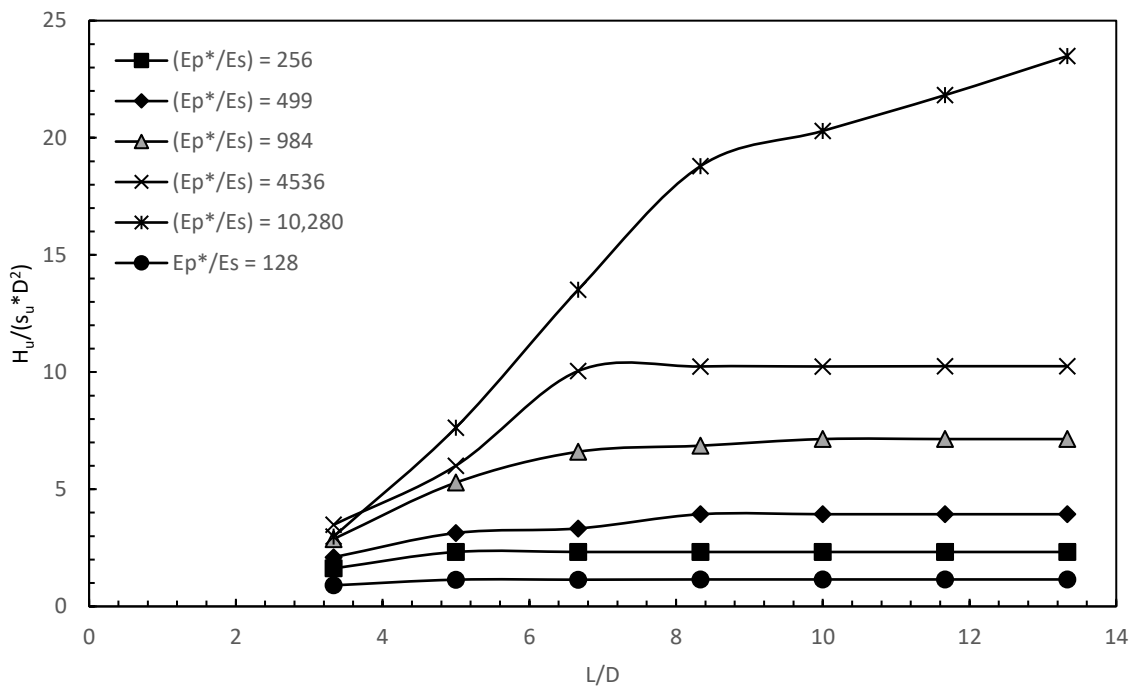


Figure 12. Normalized lateral ultimate capacity of the monopiles versus L/D for different soil profiles considered.

4.1.1. Monopile Bending Moment at Lateral Ultimate Capacity

Examining bending-moment (BM) profiles for MP at lateral ultimate capacity can aid in assessing pile behaviour and determining structural failure. Figures 13 and 14 display the bending-moment profiles for two soils, namely soil 1 and 6. Figure 13 presents the BM profile against normalized depth, l/L , for different pile lengths in a soft clay at the maximum lateral loads ($S_{u0} = 4.2$ kPa). As expected, the piles behave rigidly in all cases, with the pile showing a toe kick in behavior and zero BM at the pile toe. In contrast, the

piles behave rigidly for small L values up to 40 m and start to show a negative moment when the soil profile is stiff as shown in Figure 14 ($S_{u0} = 354 \text{ kPa}$).

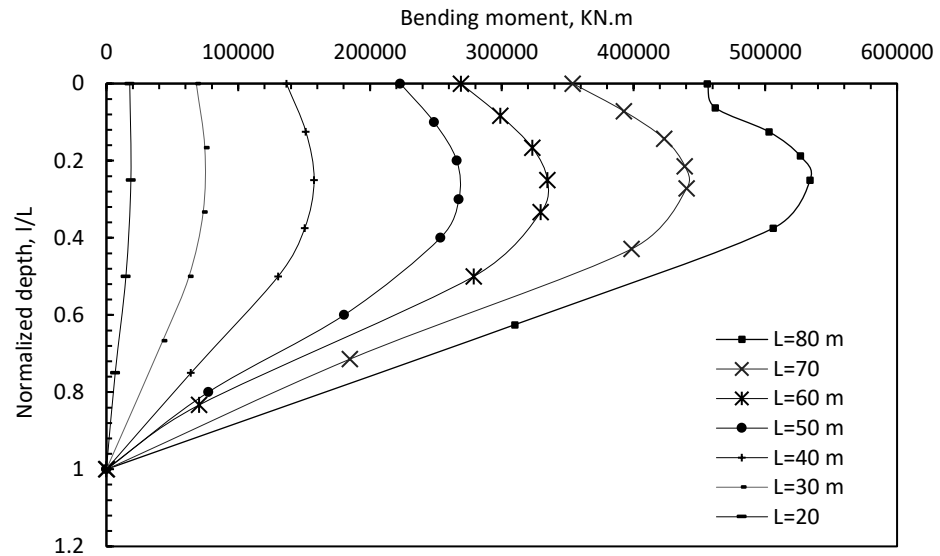


Figure 13. Bending moment versus normalized depth for MP in soft soil (clay 1) profile.

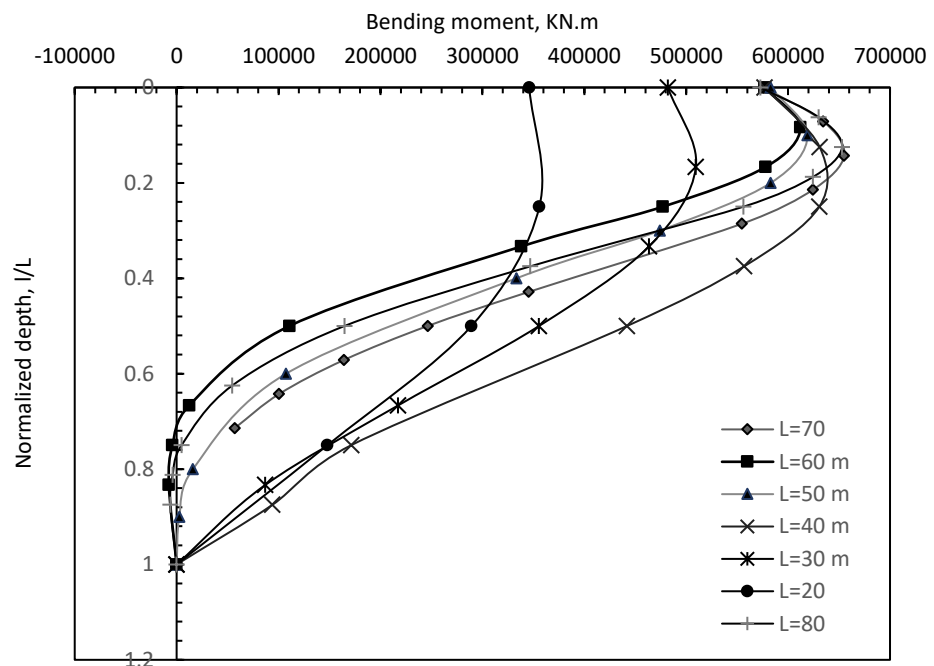


Figure 14. Bending moment versus normalized depth for stiff soil (clay 6) profile.

4.1.2. Predictive Equations for Determining Lateral Ultimate Capacity for Monopiles

By curve fitting the data in Figure 11, equations are obtained for determining the lateral ultimate capacity of monopiles for various E_p^*/E_{50} ratios between 10,280 and 128 and L/D ratios between 3.33 and 13.33 for the case of e/D_t of 6.83. Second-order polynomials were chosen based on the regression analyses. Equations (6)–(11) describe the ultimate capacity of MP in a clayey medium under eccentric loading of $e/D_t = 6.83$ as representative of medium-depth water (i.e., water depth between 10–40 m). Figure 15 demonstrates excellent agreement between the predicted ultimate-capacity-employing Equations (6)–(11) and those calculated from the FE analysis ($0.91 < R^2 < 0.999$).

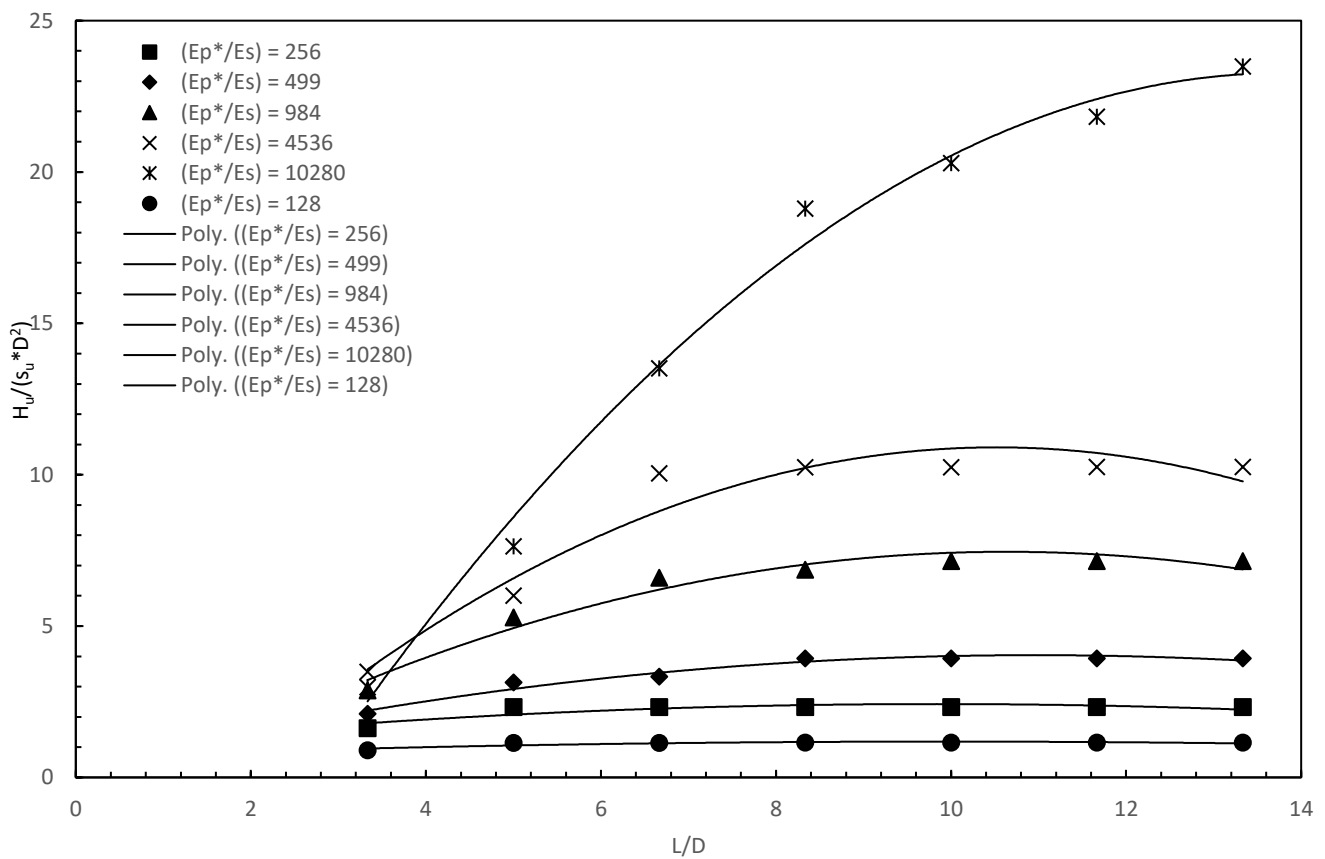


Figure 15. Comparison of predicted and calculated ultimate capacity.

For $(E_p^*/E_{50} = 10,280)$:

$$\frac{H_u}{S_u D^2} = -0.1897 * \left(\frac{L}{D}\right)^2 + 5.2326 * \left(\frac{L}{D}\right) - 12.823 \quad (R^2 = 0.9916) \quad (6)$$

For $(E_p^*/E_{50} = 4536)$:

$$\frac{H_u}{S_u D^2} = -0.1161 * \left(\frac{L}{D}\right)^2 + 2.5244 * \left(\frac{L}{D}\right) - 3 \quad (R^2 = 0.949) \quad (7)$$

For $(E_p^*/E_{50} = 984)$:

$$\frac{H_u}{S_u D^2} = -0.0796 * \left(\frac{L}{D}\right)^2 + 1.6913 * \left(\frac{L}{D}\right) - 1.5355 \quad (R^2 = 0.9583) \quad (8)$$

For $(E_p^*/E_{50} = 499)$:

$$\frac{H_u}{S_u D^2} = -0.0315 * \left(\frac{L}{D}\right)^2 + 0.6905 * \left(\frac{L}{D}\right) + 0.256 \quad (R^2 = 0.9633) \quad (9)$$

For $(E_p^*/E_{50} = 256)$:

$$\frac{H_u}{S_u D^2} = -0.1203 * \left(\frac{L}{D}\right)^2 + 1.0909 * \left(\frac{L}{D}\right) \quad (R^2 = 0.9165) \quad (10)$$

For ($E_p^*/E_{50} = 128$):

$$\frac{H_u}{S_u D^2} = -0.0053 * \left(\frac{L}{D}\right)^2 + 0.1044 * \left(\frac{L}{D}\right) + 0.6661 \quad (R^2 = 0.9229) \quad (11)$$

5. Conclusions

Monopile-foundation utilisation for OWTs plays an important role in supporting the development of green electricity alternatives. Further development of OWT farms is expected to include bigger and heavier turbines, to add more electricity, in addition to being moved to deeper water locations, hence increasing loads on foundations and requiring massive foundation elements. A typical foundation system for OWTs can consume up to 40% of the initial cost with monopile diameters and depths reaching 7.8 m and 80 m, respectively. Therefore, a critical review of foundation design is needed, and optimization and innovation in this field is necessary. Although there are plenty of studies on the lateral ultimate capacity of piles, few studies exist on determining the lateral ultimate capacity for monopile foundations for wind turbines, and, therefore, the aim of this paper was to close this gap in the literature by studying their lateral ultimate capacity in cohesive soils under eccentric loading that is typical for offshore locations.

Different soil conditions were considered, and a validated FE model was employed using the hardening soil (HS) constitutive relationship with parameters calibrated and verified from field tests. Typical procedures involved creating a k_o geostatic stage followed by an installation stage, which was then used to apply displacement-controlled loading, from which generic curves and best-fit equations were established to obtain ultimate lateral capacity for the considered system. Several conclusions were drawn from the results and are discussed below:

1. The normalized ultimate capacity versus normalized stiffness of MPs showed three distinct slopes, and the normalized ultimate capacity was observed to increase significantly for E_p^*/E_{50} values less than 984 for all L/D ratios. At normalized stiffness values of more than 2000, the effects of increasing the stiffness for a given L/D ratio was small for L/D ratios less than six and was considerable for higher L/D ratios.
2. The normalized lateral ultimate capacity increase with L/D ratio was dependent on the normalized stiffness (E_p^*/E_{50}) values. At large E_p^*/E_{50} values, the piles behaved as rigid piles and linear growth of the normalized lateral ultimate capacity was observed for the L/D ratios considered herein. As normalized stiffness (E_p^*/E_{50}) values decrease below 984, the effects of L/D ratio on the lateral ultimate capacity diminish around L/D values of 5–8. These findings are better understood through inspection of the bending-moment profiles for clay soils 1 and 6.
3. Higher L/D ratios had increased normalized lateral capacity for clays 1–5. In clay 6, no effects on the normalized lateral capacity were observed with changes in L/D.
4. For clay 1, increasing L/D ratio from 3.3 to 13.3 gave substantial increases in normalized lateral ultimate capacity of more than 700%. For clay 2, a similar observation was made, however, with a lower magnitude.
5. For clays 3–4, the effects of L/D ratio on the normalized lateral ultimate capacity were noticeable, amounting to 100%. However, the increase ceased after L/D values of 8.3.
6. For clays 5–6, the effects of L/D ratio on the normalized lateral ultimate capacity were negligible due to the flexibility of the monopiles.
7. Predictive polynomials showed excellent matches with the FE data, giving promising results and paving the way for more FE-based charts for preliminary estimates of monopile lateral ultimate capacity.

Author Contributions: Y.A.A.: Conceptualization, Interpretation, Writing- Original draft preparation. M.H.E.N.: Software and supervision. T.N.: Supervision, methodology, Reviewing and Editing. J.A.B.: Supervision. All authors have read and agreed to the published version of the manuscript.

Funding: This research received no external funding.

Institutional Review Board Statement: Not applicable.

Informed Consent Statement: Not applicable.

Data Availability Statement: The data presented in this study are available in the article.

Acknowledgments: Researchers would like to thank the Deanship of Scientific Research, Qassim University for funding the publication of this project.

Conflicts of Interest: The authors declare no conflict of interest.

References

1. Alsharedah, Y.; Black, J.A.; Newson, T.; El Naggar, M.H. Centrifuge Testing of Improved Monopile Foundation for Offshore Wind Turbines. *Ocean Eng.* **2023**, *2*, 285. [CrossRef]
2. Alsharedah, Y.A. Behavior of Hybrid and Monopile Foundation Systems for OWT: Centrifuge Testing and Numerical Modelling. Doctoral Dissertation, The University of Western Ontario, London, ON, Canada, 2022; p. 8580. Available online: <https://ir.lib.uwo.ca/etd/8580> (accessed on 23 December 2022).
3. Alsharedah, Y.; Black, J.A.; Newson, T.; El Naggar, M.H. Monopile and Hybrid Foundation Comparisons under Lateral Loading. In Proceedings of the International Conference on Physical Modelling in Geotechnics (ICPMG 2022), Daejeon, Republic of Korea, 19–23 September 2022.
4. Prendergast, L.J.; Igoe, D. Examination of the reduction in natural frequency of laterally loaded piles due to strain-dependence of soil shear modulus. *Ocean Eng.* **2022**, *258*, 111614. [CrossRef]
5. National Wind Energy Associations. Offshore Wind in Europe—Key Trends and Statistics 2020. Report 2020. Available online: <https://windeurope.org/intelligence-platform/product/offshore-wind-in-europe-key-trends-and-statistics-2020/> (accessed on 29 October 2023).
6. Abdelkader, A.M. Investigation of Hybrid Foundation System for Offshore Wind Turbine. Doctoral Dissertation, The University of Western Ontario, London, ON, Canada, 2016.
7. Byrne, B.W.; Houlsby, G.T. Foundations for Offshore Wind Turbines. *Philos. Trans. R. Soc. Lond. Ser. A Phys. Eng. Sci.* **2003**, *361*, 2909–2930. [CrossRef] [PubMed]
8. El-Marassi, M. *Investigation of Hybrid Monopile-Footing Foundation Systems Subjected to Combined Loading*; The University of Western Ontario: London, ON, Canada, 2011.
9. Poulos, H.G. Tall building foundations: Design methods and applications. *Innov. Infrastruct. Solut.* **2016**, *1*, 10. [CrossRef]
10. Byrne, B.W.; McAdam, R.; Burd, H.J.; Houlsby, G.T.; Martin, C.M.; Zdravković, L.; Taborda DM, G.; Potts, D.M.; Jardine, R.J.; Sideri, M.; et al. New design methods for large diameter piles under lateral loading for offshore wind applications. *Front. Offshore Geotech.* **2015**, *1*, 705–710.
11. Bisoi, S.; Haldar, S. Dynamic analysis of offshore wind turbine in clay considering soil-monopile-tower interaction. *Soil Dyn. Earthq. Eng.* **2014**, *63*, 19–35. [CrossRef]
12. McClelland, B.; Focht, J.A., Jr. Soil modulus for laterally loaded piles. *Trans. Am. Soc. Civ. Eng.* **1958**, *123*, 1049–1063. [CrossRef]
13. PY-2014/01/14SP—SN—978-1-138-00152-7T1; Haigh, Stuart—Foundations for Offshore Wind Turbines. Available online: https://www.researchgate.net/profile/Stuart-Haigh/publication/275538646_Foundations_for_offshore_wind_turbines/links/55433ed10cf24107d3949628/Foundations-for-offshore-wind-turbines.pdf (accessed on 29 October 2023).
14. O'Neill, M.W.; Reese, L.C.; Brown, D.A. Cyclic lateral loading of a large-scale pile group. *J. Geotech. Eng.* **1987**, *113*, 1326–1343. [CrossRef]
15. Matlock, H. Correlations for Design of Laterally Loaded Piles in Soft Clay. In Proceedings of the 2nd Offshore Technology Conference, Houston, TX, USA, 22–24 April 1970; Volume 1, pp. 577–594.
16. Reese, L.C.; Cox, W.R.; Koop, F.D. Field testing and analysis of laterally loaded piles in stiff clay. In Proceedings of the 7th Offshore Technology Conference, Houston, TX, USA, 5–8 May 1975; Volume 2, pp. 671–690.
17. Byrne, B.W.; McAdam, R.; Burd, H.J.; Houlsby, G.T.; Martin, C.M.; Gavin, K.; Doherty, P.; Igoe, D.; Zdravković, L.; Taborda DM, G.; et al. Field testing of large diameter piles under lateral loading for offshore wind applications. In Proceedings of the XVI European Conference on Soil Mechanics and Geotechnical Engineering, Edinburgh, UK, 13–17 September 2015; pp. 1255–1260.
18. Philippe, J. Re-assessment of P-Y curves for soft clays from centrifuge testing and finite element modeling. In Proceedings of the Offshore Technology Conference, Houston, TX, USA, 4 May 2009. [CrossRef]
19. Meyer, B.J.; Reese, L.C. *Analysis of Single Piles under Lateral Loading*; FHWA report/TX-79/38+244-l; Center for Highway Research, University of Texas at Austin: Austin, TX, USA, 1979.
20. Lau, B. Cyclic Behaviour of Monopile Foundations for Offshore Wind Turbines in Clay. Ph.D. Dissertation, University of Cambridge, Cambridge, UK, 2015.
21. Wang, Z.; Hong, Y.; Ng CW, W.; Wang, L.Z.; Mašin, D.; He, B. Cyclic lateral response and failure mechanisms of semi-rigid pile in soft clay: Centrifuge tests and numerical modelling. *Can. Geotech. J.* **2017**, *54*, 806–824. [CrossRef]
22. Zhu, B.; Zhu, Z.; Li, T.; Liu, J.; Liu, Y. Field Tests of Offshore Driven Piles Subjected to Lateral Monotonic and Cyclic Loads in Soft Clay. *J. Waterw. Port Coast. Ocean Eng.* **2017**, *143*, 5017003. [CrossRef]

23. Heidari, M.; Jahanandish, M.; Naggar, H.E.; Ghahramani, A. Nonlinear cyclic behavior of laterally loaded pile in cohesive soil. *Can. Geotech. J.* **2014**, *51*, 129–143. [[CrossRef](#)]
24. API. *Recommended Practice for Planning, Designing, and Constructing Fixed Offshore Platforms*; API, RPT2A-WSD; American Petroleum Institute (API): Washington, DC, USA, 1993.
25. Bayton, S.; Black, J.; Klinkvort, R. Centrifuge modelling of long term cyclic lateral loading on monopiles. In *Physical Modelling in Geotechnics*, 1st ed.; Routledge: London, UK, 2018; pp. 689–694. [[CrossRef](#)]
26. Broms, B.B. Lateral Resistance of Piles in Cohesive Soils. *J. Soil Mech. Found.* **1964**, *90*, 27–64. [[CrossRef](#)]
27. Brown, D.A. Rapid lateral load testing of deep foundations. *DFI J. J. Deep Found. Inst.* **2007**, *1*, 54–62. [[CrossRef](#)]
28. Cherchia, M. Centrifuge Modeling of Hybrid Foundations for Offshore Wind Turbines. Doctoral Dissertation, Rensselaer Polytechnic Institute, Troy, NY, USA, 2016.
29. Gerolymos, N.; Giannakos, S.; Drosos, V. Generalised failure envelope for laterally loaded piles: Analytical formulation, numerical verification and experimental validation. *Géotechnique* **2020**, *70*, 248–267. [[CrossRef](#)]
30. Lehane, B.; Powrie, W.; Doherty, J. Centrifuge model tests on piled footings in clay for offshore wind turbines. In *Frontiers in Offshore Geotechnics II*; CRC Press: Boca Raton, FL, USA, 2010.
31. Powrie, W.; Daly, M.P. Centrifuge modeling of embedded retaining walls with stabilizing bases. *Geotechnique* **2007**, *57*, 485–497. [[CrossRef](#)]
32. Wang, X.; Zeng, X.; Yang, X.; Li, J. Feasibility study of offshore wind turbines with hybrid monopile foundation based on centrifuge modeling. *Appl. Energy* **2018**, *209*, 127–139. [[CrossRef](#)]
33. Zhang, G. A centrifuge study of the seismic response of pile–raft systems embedded in soft clay. *Géotechnique* **2017**, *67*, 479–490. [[CrossRef](#)]
34. Schanz, T.; Vermeer, P.A.; Bonnier, P.G. The hardening soil model: Formulation and verification. *Beyond 2000 Comput. Geotech.* **1999**, *1*, 281–296.
35. Lai, Y.; Wang, L.; Hong, Y.; He, B. Centrifuge modeling of the cyclic lateral behavior of large-diameter monopiles in soft clay: Effects of episodic cycling and reconsolidation. *Ocean. Eng.* **2020**, *200*, 107048. [[CrossRef](#)]
36. Dao, T.P.T. *Validation of PLAXIS Embedded Piles for Lateral Loading*; Delft University of Technology: Mekelweg, The Netherlands, 2011.

Disclaimer/Publisher’s Note: The statements, opinions and data contained in all publications are solely those of the individual author(s) and contributor(s) and not of MDPI and/or the editor(s). MDPI and/or the editor(s) disclaim responsibility for any injury to people or property resulting from any ideas, methods, instructions or products referred to in the content.